Journal of Power Sources 196 (2011) 820–826

Contents lists available at ScienceDirect

Journal of Power Sources

journal homepage: www.elsevier.com/locate/jpowsour

Demonstration of a micro-fabricated hydrogen storage module for micro-power systems

Xi Shan[a,*], Joe H. Payer[a], Jesse S. Wainright[b], Laurie Dudik[b]

[a] Corrosion and Reliability Engineering, Department of Chemical and Biomolecular Engineering, University of Akron, 302 Buchtel Common, Akron, OH 44325, USA
[b] Department of Chemical Engineering, Case Western Reserve University, Cleveland, OH 44106, USA

ARTICLE INFO

Article history:
Received 11 June 2010
Received in revised form 16 July 2010
Accepted 20 July 2010
Available online 30 July 2010

Keywords:
$CaNi_5$
Fuel cell
Hydrogen storage
$LaNi_{4.7}Al_{0.3}$
PEM

ABSTRACT

The objective of this work was to demonstrate a micro-fabricated hydrogen storage module for micro-power systems. Hydrogen storage materials were developed as thin-film inks to be compatible with an integrated manufacturing process. Performance and durability of storage modules were evaluated. Further, applications were demonstrated for a nickel–hydrogen battery and a micro-fabricated hydrogen–air PEM fuel cell. The ink making process, in which polymer binders and solvents were added to the palladium-treated alloys, slightly decreased the storage capacities, but had little effect on the activation properties of the treated alloys. After 5000 absorption/desorption cycles under hydrogen, the hydrogen storage capacities of the thin-film inks remained high. Absorption/desorption behavior of the ink was tested in the environment of a new type nickel–hydrogen battery, in which it would in contact with 26 wt% KOH solution, and the ink showed no apparent degradation. Storage modules were successfully used as the hydrogen source for PEM fuel cell.

1. Introduction

The development of micro-electro-mechanical system (MEMS) sensors and actuators needs an onboard power source with high energy capacity. A number of micro-power systems, such as a micro-fabricated hydrogen–air PEM fuel cell system [1], and a new kind of low pressure nickel–hydrogen battery that utilizes a metal hydride to store hydrogen, rather than a negative electrode in the nickel-metal hydride battery [2,3], are being developed. PEM fuel cell technology can provide both the steady state and pulse power required by these devices, and can be integrated with the MEMS fabrication. Due to low working pressure and limited contact with the corrosive solution, the low pressure nickel–hydrogen battery is safe and has potential long cycle life. A durable hydrogen fuel source is needed for these micro-power systems.

The electric capacity of a micro-power system is determined by the amount of fuel-hydrogen available from the hydrogen source. For the micro-power systems, a high voluminal capacity is critical. Due to the mechanical strength of the micro-power systems and the proposed working environment which is near ambient condition, the hydrogen source should absorb or release hydrogen readily under atmospheric pressure at room temperature, and the hydrogen release rate should be fast, so that the micro-power system can provide high current. Since the hydrogen source is integrated with the micro-power systems, it should be compatible with the micro-fabrication process and the working environments, such as the high humidity in the fuel cell environment or high concentration KOH in the nickel–hydrogen battery environment. For longer service life and lower cost, the hydrogen source should be reusable.

Intermetallic hydrogen storage alloys that have voluminal capacity higher than that of liquid hydrogen and proper working pressure and temperature can be identified [4]. The hydrogen in intermetallic hydrogen storage alloys can also be reversibly absorbed/desorbed at high rates. However, a common characteristic of the hydrogen storage metals and alloys is that they need high pressure hydrogen for activation before they can absorb hydrogen readily under the normal working pressure, e.g. $LaNi_{4.7}Al_{0.3}$ and $CaNi_5$ has a plateau pressure of around 0.05 MPa at room temperature, but in order to activate $LaNi_{4.7}Al_{0.3}$ and $CaNi_5$ in short time, a pressure of 1–3 MPa is needed. These pressures are far greater than the desired working range of the micro-power systems.

By modifying the surface composition/structure of the hydrogen storage alloys, the activation pressure can be lowered. The surface modification can be chemical treatment [5,6], coating with Pt group metals by electrodeless plating [7], or mechanical grinding the intermetallic alloys with catalysts to nano-size particles [8–10].

Based on the hydrogen storage capacity and working pressure, $LaNi_{4.7}Al_{0.3}$ and $CaNi_5$ were selected for the hydrogen storage module for the micro-power systems. However, the as-received $LaNi_{4.7}Al_{0.3}$ and $CaNi_5$ could not be activated easily under ambient pressure and temperature. The activation behaviors of $LaNi_{4.7}Al_{0.3}$ and $CaNi_5$ were improved greatly by Pd-treatment composed

* Corresponding author. Tel.: +1 330 972 2968; fax: +1 330 972 5141.
E-mail address: shan@uakron.edu (X. Shan).

0378-7753/$ – see front matter © 2010 Elsevier B.V. All rights reserved.
doi:10.1016/j.jpowsour.2010.07.077

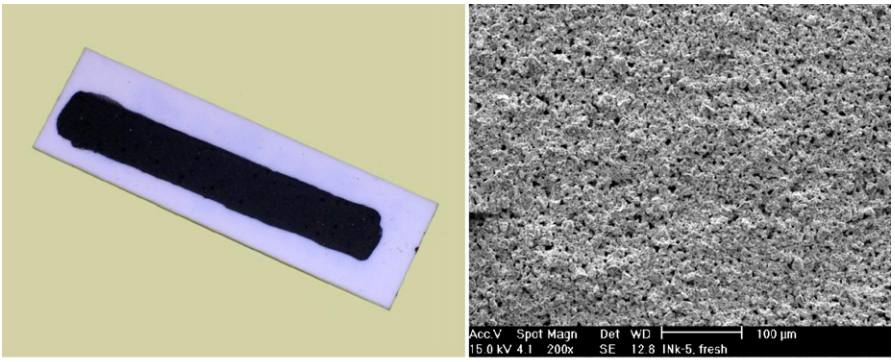

(a) overview (b) high magnification

Fig. 1. Hydrogen storage module fabricated from a thin-film ink, 10 wt% palladium-treated $LaNi_{4.7}Al_{0.3}$ PEO binder. (a) Overview and (b) high magnification.

of grinding with small amount of palladium [11,12]. The Pd-treated alloys could absorb hydrogen readily under atmospheric hydrogen at room temperature even after being exposed to air for more than two years [11,12]. The palladium-treated hydrogen storage alloy could also keep the ready activation property and air exposure durability after the micro-fabrication process which involved mixing the palladium-treated alloy with polymer binder and solvent and baking at high temperature. The pressure–composition isotherm (PCI) of the Pd-treated alloys was not affected micro-fabrication process. The detailed results on the effect of micro-fabrication process and the performance of the inks made with the Pd-treated alloys are reported somewhere else [13].

The mechanism of the increased performance and durability is hydrogen spillover, and has been presented [14]. In this work, the use of the palladium-treated alloys for hydrogen source along with a new type nickel–hydrogen battery and a PEM fuel cell was demonstrated. The objective of this work was to demonstrate a hydrogen storage module for an onboard electrical power source for micro-power systems.

2. Materials and methods

2.1. Materials

Intermetallic alloys $LaNi_{4.7}Al_{0.3}$ and $CaNi_5$ with a particle size of around 75 μm were obtained from Ergenics Inc., Ringwood, NJ. Palladium powder with a surface area of 20 $m^2\,g^{-1}$ was obtained from Alfa Aesar. To prepare the palladium-treated alloy for the thin-film ink, the as-received $LaNi_{4.7}Al_{0.3}$ or $CaNi_5$ was mixed with palladium powder in the weight ratio of 10 vs. 1 and ground with mortar and pestle in air for 25–30 min. After grinding, the particle size of $LaNi_{4.7}Al_{0.3}$ and $CaNi_5$ was about 15 μm and 50 μm or less respectively.

The palladium-treated alloy was used in the form of thin-film ink which was made by micro-fabrication process. In the micro-fabrication process, the polymer binder was dissolved in the solvent first. After that, the proper amount of palladium-treated alloy was mixed with the solution into a uniform paste. Then the paste was uniformly put on an alumina ceramic slide as a thin film. The size of the ceramic slide was 50 mm × 12.5 mm. The solvent was removed by drying the ink in air or baking in an oven. The final form of the ink was composed of a mixture of the Pd-treated alloy and polymer binder as a 0.2–0.5 mm thick thin film on a ceramic slide, and the area covered by the ink was around 3 cm^2. A prepared thin-film ink sample is shown in Fig. 1. The polymer binders studied were: polyethylene oxide (PEO) and polyvinylidene fluoride (PVDF). The PEO ink contained 0.5 wt% PEO binder, and the PVDF ink contained 2 wt% PVDF binder.

To be close to the practical application, general grade hydrogen was used in the hydrogen absorption tests and the composition was: H_2 99.95%, O_2 10 ppm, N_2 400 ppm and H_2O 32 ppm.

2.2. Methods

The hydrogen absorption/desorption tests were carried on a 304 stainless steel Sievert's apparatus with a total volume of 192 cm^3. Hydrogen absorption/desorption cycle tests were performed on a modified Sievert's apparatus which had four independently controlled sample containers and up to four samples could be tested simultaneously. The schedule in the cycle test was 10-min absorption under approximately an initial applied pressure of 110 kPa followed by 10-min desorption in vacuum and repeat. During the absorption process, the pressure change was less than 5% of the initial applied pressure. After every 1000 cycles, the hydrogen absorption of each sample was checked, and then the cycle test was paused and the samples were taken out from the cyclic test instrument for ink morphology and microstructure analysis. The total air exposure time during these examination periods was between 24 and 72 h.

When the palladium-treated alloys are used in a new type nickel–hydrogen battery [2], it is possible that the KOH solution in the battery can leak to the hydrogen storage module. A KOH soak test was performed to simulate actual condition in the battery. The test setup is shown in Fig. 2. Celgard® 3400 micro-porous membrane was used to hold the KOH solution. The membrane contained 37% porosity with a pore size of 0.117 μm × 0.042 μm and has a thickness of 25 μm. The Celgard® 3400 porous membrane was dipped into a 26 wt% KOH solution for 30 s, then the extra solution

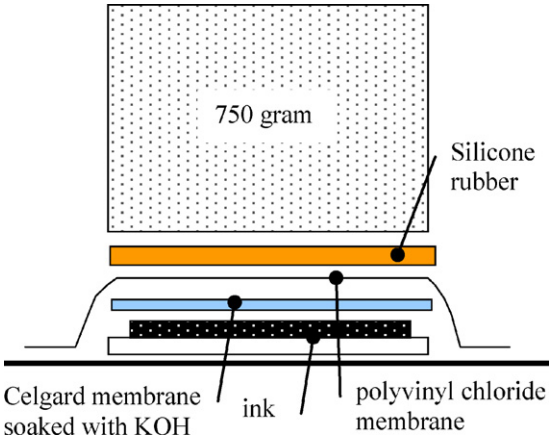

Fig. 2. KOH soak test of thin-film ink with Celgard® 3400 micro-porous membrane.

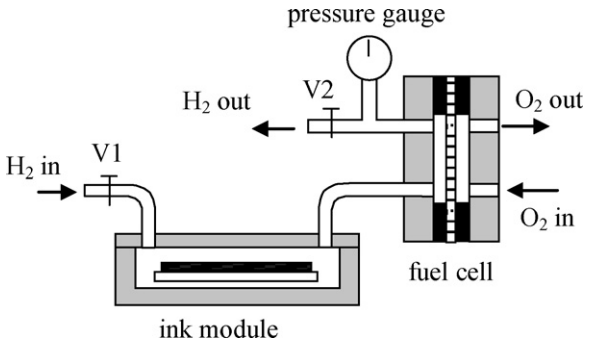

Fig. 3. Measurement of PEM fuel cell performance powered with thin-film ink.

on the surface of the membrane was removed. The soaked membrane, which contained 33 wt% KOH solution, was put on top of the thin-film ink. To prevent the evaporation of the KOH solution, a plastic film was used to cover the thin-film ink and Celgard® 3400 porous membrane. A weight of 750 g was added on the top of the ink to make a close contact between porous membrane and the ink. The soaked porous membrane was replace with a new soaked membrane after 48 h, the soaked porous membrane was replace one more time after another 24 h. The total time that the ink was in contact with the soaked porous membrane was 92 h. After the KOH soak test, the hydrogen absorption behavior of the ink was tested. The tested ink was the Pd-treated $LaNi_{4.7}Al_{0.3}$ PDVF ink, and the weight of the hydrogen storage alloys was 0.11 g.

The electrochemical performances of a PEM fuel cell with the thin-film inks as the hydrogen source were measured. Fig. 3 shows the fuel cell performance test setup. The total inner volume of the ink module and the fuel cell was 18 cm^3. In the test, a Nafion® membrane was used in the fuel cell, and the area of the electrodes was 1 cm^2. A MKS-122BA-10000 pressure gauge was connected to the hydrogen outlet of the fuel cell to monitor the hydrogen pressure inside the fuel cell. The leakage rate of the fuel cell test module was controlled to be less than 0.4 kPa h^{-1} under 107 kPa hydrogen. This was on the same level as the hydrogen permeation rate through the Nafion® membrane. Before the electrochemical test, the system was purged with 106.7 kPa hydrogen on the anode side and oxygen on the cathode side for at least 1 h so that the hydrogen storage inks were fully charged. After purging, V1 and V2 in Fig. 3 were closed, and hydrogen from the inks in the hydrogen storage ink module fueled the fuel cell. The fuel cell was galvanostatically or potentiodynamically polarized by an EG&G 273A potentiostat. The software used to control the potentiostat was Corrware®.

The scanning electron microscopy (SEM) analysis was performed on Philips XL-30.

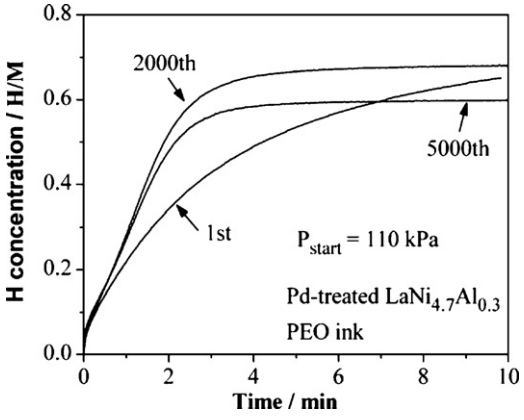

Fig. 4. Effect of absorption/desorption cycles on the absorption of Pd-treated $LaN_{4.7}Al_{0.3}$ PEO ink.

3. Results

3.1. Effect of absorption/desorption cycle on the hydrogen absorption of the ink

Fig. 4 shows the effect of hydrogen absorption/desorption cycle test on absorption process of palladium-treated $LaNi_{4.7}Al_{0.3}$ PEO ink. The absorption rate increased with increasing the cycle number in the first 2000 absorption/desorption cycles, from 2000 to

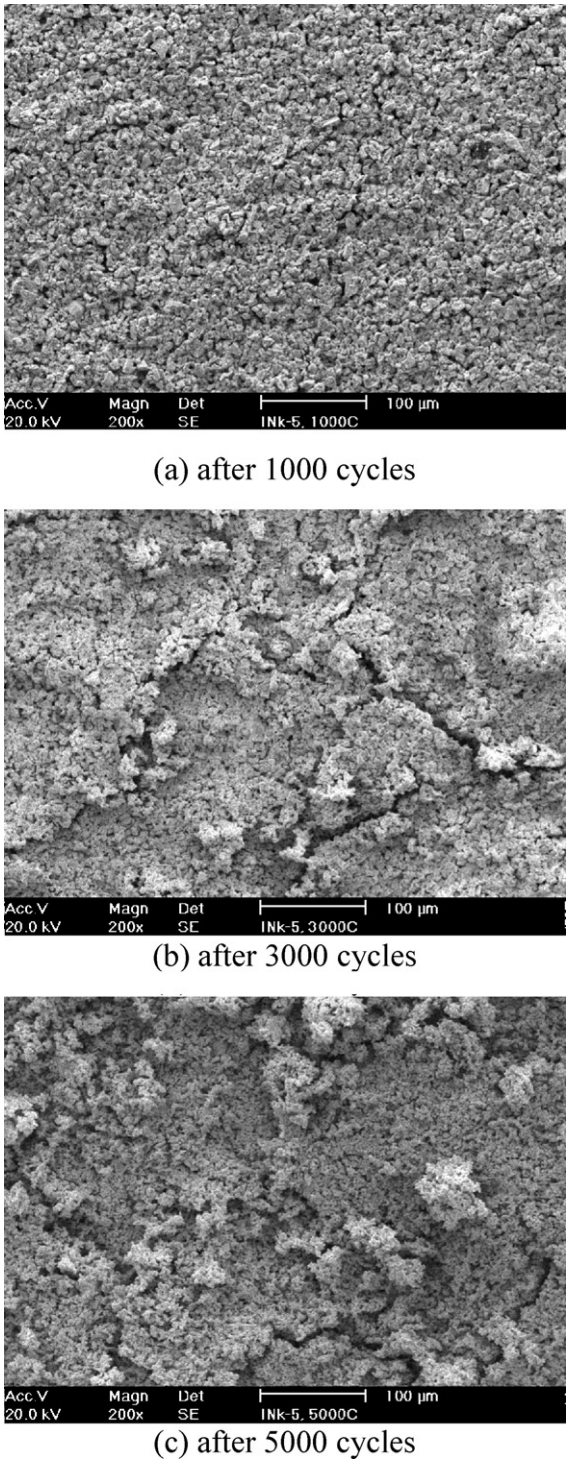

Fig. 5. Effect of absorption/desorption cycles on the morphology of Pd-treated $LaNi_{4.7}Al_{0.3}$ PEO ink. (a) After 1000 cycles, (b) after 3000 cycles and (c) after 5000 cycles.

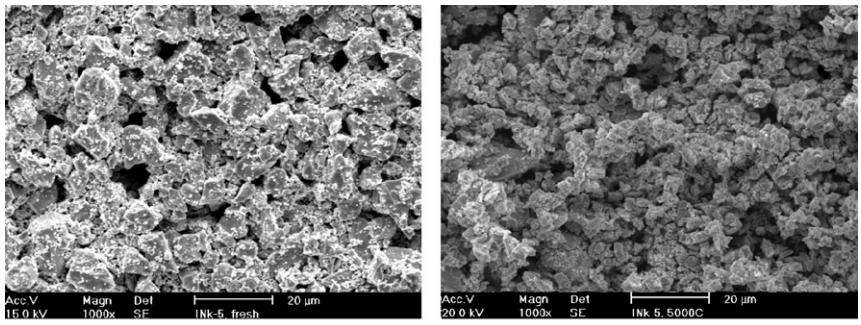

(a) before test (b) after 5000 cycles

Fig. 6. Particle size changes of $LaNi_{4.7}Al_{0.3}$ before and after cycle test. (a) Before test and (b) after 5000 cycles.

5000 cycles, the absorption/desorption cycle number has almost no effect on the absorption rate. Overall, after 5000 cycles of absorption/desorption test, the absorption rate increased slightly. However, the final equilibrium hydrogen decreases slightly with increasing the cycle number. After 5000 cycles, the total decrease of the hydrogen storage capacity was 14%. The reason for the decreasing with increasing the cycle number was caused by the break and air exposure after every 1000 absorption/desorption cycles, which caused the deactivation of small amount of hydrogen storage particles [13]. Similar test was also performed on palladium-treated $CaNi_5$ PEO ink, and after 5000 cycles, the capacity decrease of $CaNi_5$ was 35%. When water vapor was represented in the hydrogen gas, the degradation of the $LaNi_{4.7}Al_{0.3}$ was accelerated. The absorption/desorption cycle tests on $LaNi_{4.7}Al_{0.3}$ ink made with PDVF binder in 75% RH hydrogen showed that, after 3000 absorption/desorption cycles, the storage capacity of the ink decreased 35%. More detailed results on the effect of absorption cycle tests on the hydrogen storage performance is presented elsewhere [13].

In general, the ink integrity was not significantly affected by the hydrogen absorption/desorption cycle test. Fig. 5 shows the morphology changes of PEO ink after 1000, 3000 and 5000 absorption/desorption cycles. With increasing the absorption/desorption number, the surface roughness of the ink increased, and cracks were visible, however overall, the ink still hold overall structural integrity. After 5000 hydrogen absorption/desorption cycles, the particle size of $LaNi_{4.7}Al_{0.3}$ decreased dramatically as shown in Fig. 6. Before the test, the particle was about 15 μm, and the particle size changed to 2–3 μm after 5000 hydrogen absorption/desorption cycle test.

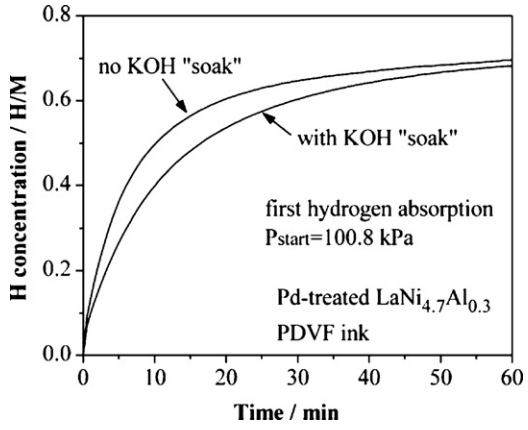

Fig. 7. Effect KOH "soaking" on the activation of Pd-treated $LaNi_{4.7}Al_{0.3}$ PDVF ink.

3.2. Nickel–hydrogen battery

For the new type low pressure nickel–hydrogen battery, the hydrogen storage module may be in contact with KOH solution. The effect of KOH exposure on performance was evaluated. Fig. 7 shows the effect of KOH soaking test on the first hydrogen absorption of

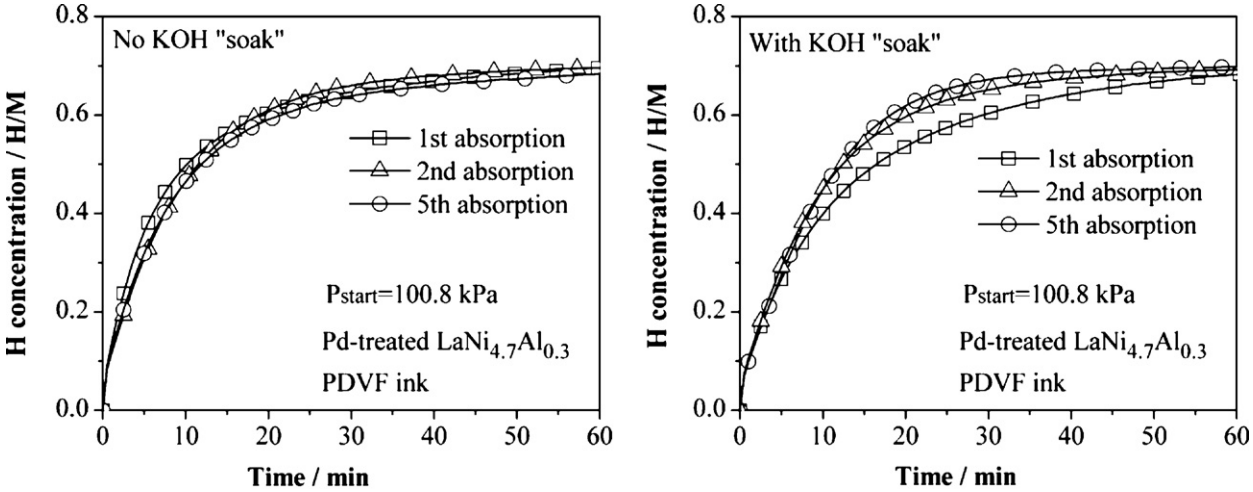

(a) No KOH "soaking" (b) with KOH "soaking"

Fig. 8. Absorption rate changes for the ink with KOH soak. (a) No KOH "soaking" and (b) with KOH "soaking"

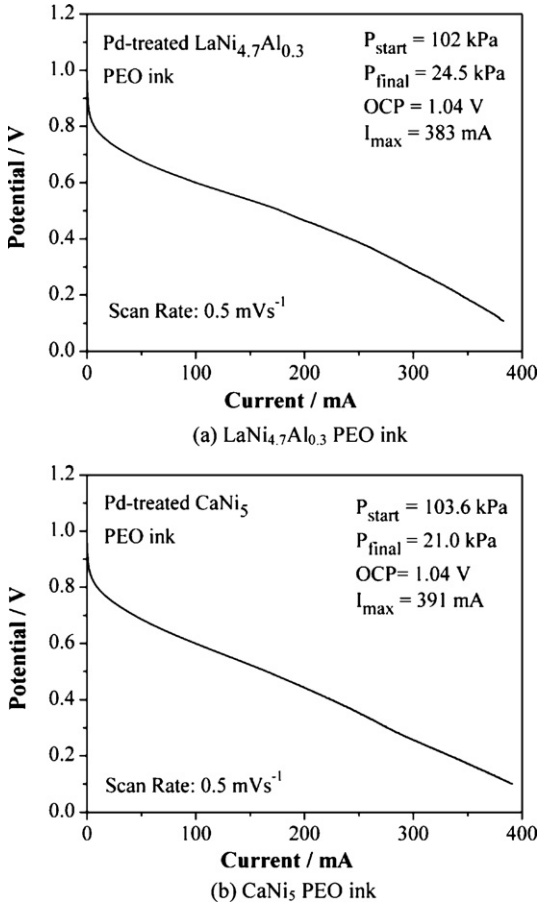

Fig. 9. Potentiodynamic performance of PEM fuel cell powered with Pd-treated (a) $LaNi_{4.7}Al_{0.3}$ and (b) $CaNi_5$ PEO ink, scan rate 0.5 mV s^{-1}.

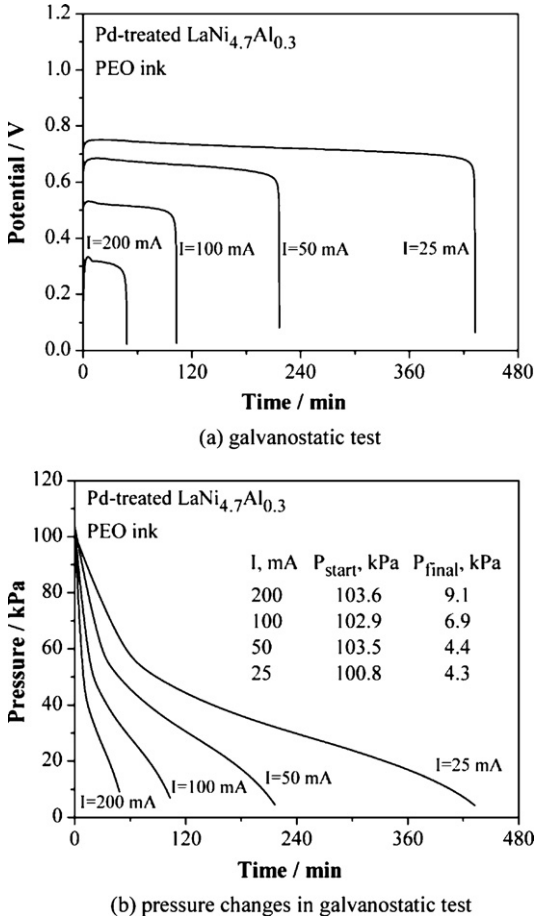

Fig. 10. Galvanostatic performance of PEM fuel cell powered with Pd-treated $LaNi_{4.7}Al_{0.3}$ PEO ink. (a) Galvanostatic test and (b) pressure changes in galvanostatic test.

palladium-treated $LaNi_{4.7}Al_{0.3}$ PDVF ink. The hydrogen absorption curve of PDVF ink from the same batch without KOH soaking is also shown in Fig. 7. The palladium-treated $LaNi_{4.7}Al_{0.3}$ PDVF ink could still absorb hydrogen readily under atmosphere hydrogen after exposing to 26 wt% KOH solution in the porous membrane for 92 h. Compared to the un-soaked ink sample, the absorption rate slightly decreased in the first absorption, but the maximum amount of hydrogen that the alloy can absorb was not affected. Fig. 8 shows the absorption curves of the soaked and un-soaked PDVF ink made with palladium-treated $LaNi_{4.7}Al_{0.3}$ for the first 5 absorption/desorption cycles. With increasing the absorption/desorption cycle number, the absorption rate of the KOH soaked sample increased, while the absorption rate of the un-soaked sample did not change much. After 5 absorption/desorption cycles, the absorption half-reaction time of the KOH soaked PDVF ink sample changed from 520 s to 400 s, and this value was close to the PDVF ink sample without KOH soaking, which was 370 s. These result shows that the effect of short-time KOH exposure on the hydrogen storage properties of the palladium-treated $LaNi_{4.7}Al_{0.3}$ was small. The contact with KOH solution slightly slowed down the hydrogen absorption rate of the PDVF ink made with palladium-treated $LaNi_{4.7}Al_{0.3}$ in the first absorption, but the effect was not permanent, and could be recovered within a few hydrogen absorption/desorption cycles.

3.3. Fuel cell performance

The combined hydrogen storage module and PEM fuel cell system performance was measured by potentiodynamic polarization and galvanostatic polarization. Fig. 9 shows the potentiodynamic polarization results of the PEM fuel cell with the palladium-treated $LaNi_{4.7}Al_{0.3}$ PEO ink and palladium-treated $CaNi_5$ PEO ink as the hydrogen source. Three inks were used as the hydrogen sources, and the total weight of the Pd-treated $LaNi_{4.7}Al_{0.3}$ and Pd-treated $CaNi_5$ were 0.54 g and 0.53 g respectively. When the final potential 0.1 V was reached, the current increased to 383 mA for $LaNi_{4.7}Al_{0.3}$ PEO ink and 370 mA for $CaNi_5$ PEO ink. Due to the consumption of the hydrogen gas, with the increase of the electric current, the hydrogen pressure in the system decreased. According to the equation $I = E/R$, the total resistance of the fuel cell was about 1.5–1.8 Ω for both tests.

Fig. 10 shows the galvanostatic test results of the fuel cell and the pressure changes when palladium-treated $LaNi_{4.7}Al_{0.3}$ PEO ink was used as the hydrogen source. Fig. 11 shows the corresponding results of palladium-treated $CaNi_5$ PEO ink. For both samples, under each test current, the potential kept almost constant during the tests. When the hydrogen pressure reached 7–8 kPa, there was a sharp drop in the potential. This was caused by the limited hydrogen transport which could not provide enough hydrogen flux to maintain the current. At the start of each test, the hydrogen pressure was above the desorption plateau pressure of the alloy, and little hydrogen gas was released from the ink. In this stage, the pressure decrease was mainly caused by the consumption of gaseous hydrogen in the system. When more and more hydrogen was consumed, the hydrogen pressure decreased to the plateau region of the alloy, and in this region, hydrogen comsumed by the fuel cell was primarily supplied by the desorption from the ink. The hydrogen desorptionslowed the pressure decrease, and the slope of pressure–time curve is small. As the pressure curves show, the pres-

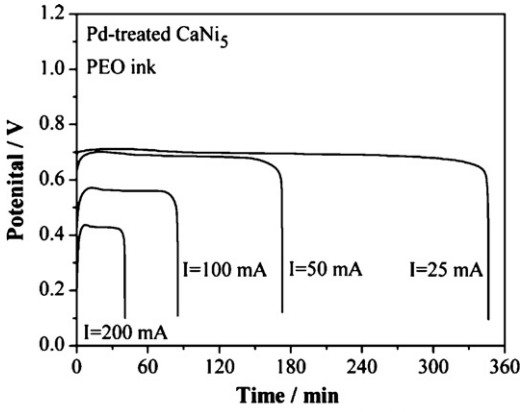

(a) potential changes with time

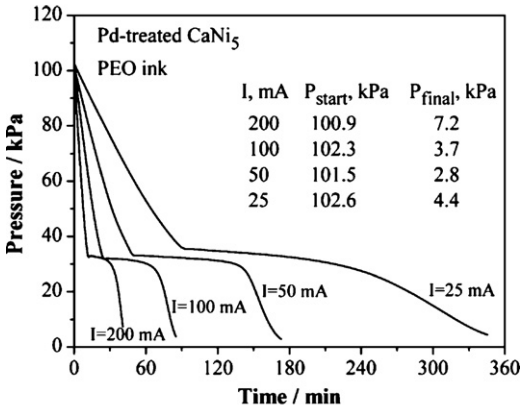

(b) pressure changes with time

Fig. 11. Galvanostatic performance of PEMFC powered with Pd-treated $CaNi_5$ ink. (a) Potential changes with time and (b) pressure changes with time.

sure changes with time in the galvanostatic tests are similar to that of the pressure–composition isotherm (PCI) curve of corresponding alloys [13].

The final hydrogen pressure depends on the galvanostatic current and increases with increasing the polarization current. For the test with 200 mA current, the final hydrogen pressure was 7.3 kPa, while for the test with 25 mA polarization current, the pressure decreased to 4 kPa. The $CaNi_5$ has a flatter plateau region than $LaNi_{4.7}Al_{0.3}$, so the pressure–time slopes of $CaNi_5$ ink are much smaller than that of $LaNi_{4.7}Al_{0.3}$. The fuel cell worked well even when the galvanostatic current was 200 mA, i.e. the hydrogen storage module was able to supply sufficient fuel.

4. Discussion

The equilibrium hydrogen concentration of $LaNi_{4.7}Al_{0.3}$ under 102.7 kPa hydrogen is 0.75 H/M, so the maximum electric capacity of 1 g ink can provide is 279 mAh g^{-1}. The loss due to the hydrogen leakage was negligible. From the galvanostatic tests of $LaNi_{4.7}Al_{0.3}$, the total capacity provided by the fuel is shown in Table 1. Because the hydrogen provided by the gaseous hydrogen in the system (the gaseous hydrogen has a volume of 18 cm^3 that corresponds to an electrical capacity of 40 mAh) and by the metal hydride is not distinguishable, both are used in the calculation of hydrogen efficiency. The energy density in Table 1 is calculated using following equation:

$$\text{Wh kg}^{-1} = (\text{Ah}_{\text{total}} - \text{Ah}_{\text{gas}}) \times \frac{V_{\text{cell}}}{w}$$

where w is the weight of $LaNi_{4.7}Al_{0.3}$.

The efficiency of the hydrogen increases as the current decreases. With high current, a high hydrogen flux is required. So even though there is hydrogen in the alloy, if the hydrogen cannot be released fast enough, it cannot be used by the fuel cell, this lowers the efficiency of hydrogen.

The energy density results show, the energy density per unit weight of the $LaNi_{4.7}Al_{0.3}$ ink is higher than that of nickel-metal hydride battery (95 Wh kg^{-1}), and close to that of rechargeable lithium ion battery (175 Wh kg^{-1}) [15]. However, this comparison considers only the weight of $LaNi_{4.7}Al_{0.3}$. In practice, the energy density of the fuel cell system depends on the design of the entire system.

The hydrogen storage capacity H/M of $CaNi_5$ is similar to that of $LaNi_{4.7}Al_{0.3}$, under 102.6 kPa hydrogen, and $CaNi_5$ can store 0.77 H/M hydrogen. The capacity that the $CaNi_5$ ink can provide if the hydrogen can be fully released is 375 mAh g^{-1}.

From the galvanostatic tests of $CaNi_5$ ink, the power, total capacity provided by the fuel cell and the capacity loss due to hydrogen leak under each test current are shown Table 2, the calculation procedure is the same as used for the $LaNi_{4.7}Al_{0.3}$ module.

The calculation of hydrogen efficiency is based on the maximum hydrogen available in $CaNi_5$ at atmospheric pressure. Compared with the hydrogen efficiency with that of $LaNi_{4.7}Al_{0.3}$, $CaNi_5$ has much lower hydrogen efficiency. The $CaNi_5$ can absorb more hydrogen per unit weight than $LaNi_{4.7}Al_{0.3}$, but its first plateau pressure is about 1.3 kPa at room temperature. This hydrogen pressure is too low for the fuel cell to use, and this makes the hydrogen efficiency much lower than that of $LaNi_{4.7}Al_{0.3}$.

For each type of ink, total three ink slides were used in the fuel cell tests, and each ink has an covered surface area of around 3 cm^2 with a thickness of around 0.2–0.5 mm, and the total hydride-covered surface area was around 9 cm^2, the Nafion® membrane in

Table 1
Galvanostatic results of $LaNi_{4.7}Al_{0.3}$ PEO ink ($LaNi_{4.7}Al_{0.3}$ weight: 0.54 g).

Current (mA)	Potential (V)	Power (mW)	Total capacity (mAh)	H_2 efficiency	Energy density (Wh kg^{-1})
25	0.72	18	180	94%	187
50	0.66	33	180	94%	171
100	0.51	51	172	90%	125
200	0.31	62	161	84%	70

Table 2
Galvanostatic results of $CaNi_5$ PEO ink ($CaNi_5$ weight: 0.53 g).

Current (mA)	Potential (V)	Power (mW)	Total capacity (mAh)	H_2 efficiency	Energy density (Wh kg^{-1})
25	0.69	17	144	61%	135
50	0.68	34	144	61%	133
100	0.56	56	142	61%	108
200	0.43	86	136	60%	78

the fuel cell was 1 cm^2, so the area ratio of the hydride ink to the PEM fuel cell membrane was 9 vs. 1.

5. Conclusion

1. The palladium-treated intermetallic hydrogen storage alloys is compatible with the thin-film ink preparing process. The think-film inks made with the palladium-treated alloys can absorb hydrogen readily under atmospheric hydrogen.
2. The contact with 26 wt% KOH solution slightly decreased the absorption rate in the first hydrogen absorption, but the absorption rate can be recovered after a few cycles of absorption and desorption.
3. The thin-film ink can keep its structural integrity after 5000 absorption/desorption cycles. The change of storage capacity with increasing the cycle number is determined by the property of the hydrogen storage alloy and the testing environment. With the existence of water vapor in the hydrogen, the degradation is accelerated.
4. Both palladium-treated $LaNi_{4.7}Al_{0.3}$ and $CaNi_5$ can be used as the hydrogen source for the micro-fabricated power systems. With a current provided by these two alloys can be higher than the requirement of the micro-fabricated PEM fuel cell. The efficiency of hydrogen provided by $LaNi_{4.7}Al_{0.3}$ can be higher than 90% at room temperature.
5. Due to the low pressure of the first plateau of $CaNi_5$, not all the hydrogen in $CaNi_5$ can be used by the fuel cell at room temperature. This leads to the low hydrogen efficiency of $CaNi_5$ module compared to the $LaNi_{4.7}Al_{0.3}$ module.
6. By monitoring the hydrogen pressure, the remaining amount of hydrogen can be determined. Hence the remaining power capacity of the fuel cell power system can be monitored.

Acknowledgements

This work was supported in part by the National Institutes of Health NINDS Grant No. NS-041809 and NIBIB Grant No. EB-001740. Joe H. Payer and Xi Shan acknowledge the collaboration and support of their colleagues at Case Western Reserve University.

References

[1] J.S. Wainright, R.F. Savinell, C.C. Liu, M. Litt, Electrochim. Acta 48 (2003) 2869.
[2] W.G. Tam, J.S. Wainright, J. Power Sources 165 (2007) 481.
[3] W.G. Tam, J.S. Wainright, ECS Trans. 1 (2006) 1.
[4] G. Sandrock, J. Alloys Compd. 293 (1999) 877.
[5] X.L. Wang, S. Suda, Z. Phys. Chem. 183 (1994) 385.
[6] X.L. Wang, S. Suda, J. Alloys Compd. 194 (1993) 73.
[7] D.B. Willey, D. Pederzolli, A.S. Pratt, J. Swift, A. Walton, I.R. Harris, J. Alloys Compd. 330–332 (2002) 806.
[8] L. Zaluski, A. Zaluska, J.O. Strom-Olsen, J. Alloys Compd. 253–254 (1997) 70.
[9] W. Oelerich, T. Klassen, R. Bormann, J. Alloys Compd. 322 (2001) L5.
[10] L. Zaluski, A. Zaluska, P. Tessier, J. Mater. Sci. 31 (1996) 695.
[11] X. Shan, J.H. Payer, J. Wainright, J. Alloys Compd. 426 (2006) 400.
[12] X. Shan, J.H. Payer, J. Wainright, J. Alloys Compd. 430 (2007) 262.
[13] X. Shan, J.H. Payer, J. Wainright, L. Dudik, J. Power Sources 196 (2011) 827–834.
[14] X. Shan, J.H. Payer, W.D. Jennings, Int. J. Hydrogen Energy 34 (2009) 363.
[15] R.J. Brodd, K.R. Bullock, J. Electrochem. Soc. 151 (2004) k1.